Accepted Manuscript

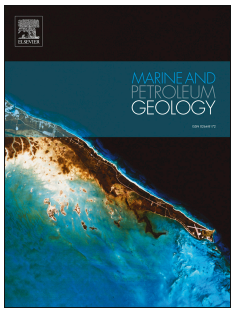

Recurrent slope failure and submarine channel incision as key factors controlling reservoir potential in the South China Sea (Qiongdongnan Basin, South Hainan Island)

Wei Li, Tiago M. Alves, Shiguo Wu, David Völker, Fang Zhao, Lijun Mi, Achim Kopf

PII: S0264-8172(15)00075-6

DOI: 10.1016/j.marpetgeo.2015.02.043

Reference: JMPG 2175

To appear in: *Marine and Petroleum Geology*

Received Date: 3 May 2014

Revised Date: 5 February 2015

Accepted Date: 24 February 2015

Please cite this article as: Li, W., Alves, T.M., Wu, S., Völker, D., Zhao, F., Mi, L., Kopf, A., Recurrent slope failure and submarine channel incision as key factors controlling reservoir potential in the South China Sea (Qiongdongnan Basin, South Hainan Island), *Marine and Petroleum Geology* (2015), doi: 10.1016/j.marpetgeo.2015.02.043.

This is a PDF file of an unedited manuscript that has been accepted for publication. As a service to our customers we are providing this early version of the manuscript. The manuscript will undergo copyediting, typesetting, and review of the resulting proof before it is published in its final form. Please note that during the production process errors may be discovered which could affect the content, and all legal disclaimers that apply to the journal pertain.

ACCEPTED MANUSCRIPT

Recurrent slope failure and submarine channel incision as key factors controlling reservoir potential in the South China Sea (Qiongdongnan Basin, South Hainan Island)

Wei Li [a, c], Tiago M. Alves [b], Shiguo Wu [a, e]*, David Völker [c], Fang Zhao [a], Lijun Mi [d], Achim Kopf [c]

[a] Key Laboratory of Marine Geology and Environment, Institute of Oceanology, Chinese Academy of Sciences, Qingdao, China
[b] 3D Seismic Lab. School of Earth and Ocean Sciences, Cardiff University, Main Building, Park Place, Cardiff, CF10 3AT, United Kingdom
[c] MARUM, Center for Marine Environmental Sciences, University of Bremen, Bremen, Germany
[d] Department of Exploration, CNOOC, Beijing 100010, China
[e] Sanya Institute of Deep Sea Science and Engineering, Chinese Academy of Sciences, Sanya 572000, China
E-mail address: swu@sidsse.ac.cn

Abstract
High-resolution multi-beam bathymetry, 3D and 2D seismic reflection profiles from the South China Sea are used to investigate the morphology, characteristics, origin and implications to petroleum systems of recurrent slope failure in the Qiongdongnan Basin, northern South China Sea. Seven Late Miocene-Holocene mass-transport deposits (MTDs) and numerous submarine canyons were identified on the continental slope and rise. Providing new insights on the evolution of an enigmatic region of the South China Sea, this paper defends that the interpreted MTDs were caused by a combination of high sedimentation rates and local tectonic uplift. By comparing the stratigraphy of the study area with local sea-level curves, we show that a significant portion of shelf-edge deposits effectively bypassed most of the continental slope during the Miocene-Quaternary to accumulate as large MTDs on its lower part (i.e. on the 'basin-floor'), independently of sea-level changes. Our work has implications to the current sequence stratigraphic models for continental margins, and sheds new light on the reservoir potential of Miocene units in the South China Sea. Hence, regions where base-of-slope fans are expected to occur are, in the study area, occupied by large-scale recurrent MTDs sourced from the shelf edge. Stratigraphically, recurrent slope instability resulted: a) in abrupt episodes of accommodation space creation on the shelf-edge, b) on a moderate reduction in accommodation space at the base of the continental slope, and c) in a complete separation between shelf and distal slope depositional systems, with most stratigraphic markers on 3D seismic data being diachronous across the continental margin. As MTDs also comprise the bulk of channel-fill deposits in large submarine canyons, we propose that the reservoir potential of channel-fill deposits in the South China Sea is closely dependent on the nature of the sediment (i.e. net-to-gross ratio) eroded and transported by these same MTDs.

Keywords: Continental slope; submarine landslides; mass-transport deposits; South China Sea; sediment bypass; petroleum systems.

1.Introduction

Sequence stratigraphy comprises the study of facies relationships and stratal architectures within known chronological frameworks, which are normally delimited on seismic and borehole data by unconformities (and correlative surfaces) of regional expression (Catuneanu et al., 2009). However, sequence stratigraphic analyses on new exploration prospects are seldom undertaken using extensive datasets, relying instead on the interpretation of seismic data complemented (when possible) with wireline and lithological information. Seismic data also images stratal architectures that are vertically separated only within the resolution limits of the seismic data, and does not resolve subtle features such as condensed sequences and high-frequency units, particularly at greater depths of investigation (Catuneanu et al., 2009).

Trying to address these caveats, multiple standardized schemes, or stratigraphic models, have been proposed in the literature, from which the most widely known are Galloway (1979), van Wagoner et al. (1990) and, more recently, Catuneanu et al. (2009). These sequence stratigraphic models assume the existence of four main genetic types of deposits: aggrading, normal regressive, forced regressive and transgressive (see also Hunt and Gawthorpe, 2000). These genetic types are mainly controlled by relative base-level changes, and do not necessarily take into account tectonic and morphological aspects of the continental margin where strata accumulates. This poses a second important limitation when interpreting continental margins around the world, particularly those on which slope instability events are common, and complex depositional systems establish the link between deposition in shelf-edge regions and the lower slope (e.g. ‘base-of-slope fans' according to van Wagoner et al., 1990). The complex way in which erosional and depositional processes interact in time and space on continental margins resulted in their classification as Exponential, Gaussian and Linear by Adams and Schlager (2000). However, most sequence stratigraphic models do not take into account the morphological variability proposed by Adams and Schlager (2000) which, as shown in this paper, can impose significant controls on the type of depositional facies expected in ‘base-of-slope’ deposits.

The term mass-transport deposit (MTD) is used in this work to describe all kinds of gravity-induced deposits transported downslope including debris flows, debris avalanches, slumps and slides, with the exception of turbidity currents (Moscardelli and Wood, 2008). MTDs play an important role in reshaping the morphology of continental margins and controlling the sedimentary architectures of sedimentary basins (Posamentier and Kolla, 2003; Gee et al., 2006; Moscardelli et al., 2006; Moscardelli and Wood, 2008). They reflect processes capable of transporting large amounts of sediment onto the deeper parts of continental margins (Weimer, 1989; Frey-Martínez et al., 2005; Gee et al.,

ACCEPTED MANUSCRIPT
2006; Masson et al., 2006; Lee et al., 2007; Moscardelli and Wood, 2008; Bull et al., 2009) and comprise heterogeneous volumes of failed sediment of distinct lithologies and degrees of internal disaggregation (Alves et al., 2014). Furthermore, MTDs comprise some of the most important near-seafloor geohazards, posing a direct threat to deep-water equipment and engineering infrastructure, such as pipelines and communication lines (Locat et al., 2002; Krastel et al., 2006; Masson et al., 2006).

MTDs are ubiquitous in the northern South China Sea (Wu et al., 2011) and particular attention has recently been paid to understand the significance, distribution, and frequency of these deposits in the Qiongdongnan Basin, or the QDNB (Sun et al., 2011; Wang et al., 2013; Li et al., 2013). This renewed attention results from the discovery of hydrocarbon reservoirs, such as the Ya 13-1 gas field, in the northern part of the basin (Chen et al., 1993; He et al., 2006). Acknowledging the importance of the QDNB as a hydrocarbon producing region, this paper uses high-resolution seismic reflection data and multi-beam bathymetry data to: (1) analyse the morphology of the central part of the QDNB; (2) document the stratigraphic distribution of recurrent MTDs accumulated from the Late Miocene on the continental rise; (3) discuss the factors controlling the deposition of these MTDs, and (4) propose a depositional model for the study area, discussing the implications of our new model to petroleum systems in the QDNB. This study will be of particular significance to future risk assessments in this area, and our model is useful to better understand the recurrence of slope failure on continental margins dominated by strike-slip tectonics such as the QDNB. In fact, previous studies on MTDs have demonstrated the significance of high-resolution multi-beam bathymetry and seismic reflection data, as those used in this paper, in improving our understanding of their internal structure and depositional evolution (Gee et al., 2006; Migeon et al., 2011; Völker et al., 2011; Krastel et al., 2012; Li et al., 2014).

2. Data and methods

Multi-beam bathymetry and high-resolution 2D and 3D seismic data were used to map Miocene-Quaternary submarine landslides and study the spatial distribution of MTDs in the QDNB (Fig. 1). The two interpreted 3D seismic volumes were acquired by China National Offshore Oil Corporation (CNOOC) in 2005 (Fig. 2). The seismic volumes were processed to a main frequency bandwidth of 30-45 Hz, and Common Mid Point spacing of 12.5 m. The vertical resolution of the seismic data is ~25 m. In addition to the two 3D seismic volumes, we interpreted 20,000 km^2 of multi-beam bathymetry data acquired in 2008 within water depths ranging from 200 m to 2600 m (Fig. 2). The horizontal and vertical resolutions of the multi-beam bathymetry data are ~100 m and ~1-3.3 m, respectively. The high-resolution of the multi-beam bathymetric data allowed us to identify and analyse any submarine landslides with seafloor expression.

Based on stratigraphic and wireline log data of Well LS33-1 (Figs. 3 and 4), main seismic reflections were identified and mapped using standard industry interpretation software. The ages of seismic surfaces were based on stratigraphy from Well LS33-1 and on previous research results (Wu et al., 2014). Seven main regional stratigraphic horizons T70 (29.3 Ma), T60 (23.3 Ma), T50 (15.5 Ma), T40 (10.5 Ma), T30 (5.5 Ma), T20 (1.9 Ma), and the seafloor, were therefore identified and tied to Well LS33-1 (Figs. 3 and 4). Post-rift sequences in deep-water regions of the QDNB chiefly consist of fine-grained hemipelagic sediments. The drilling core and logging data from Well LS33-1 reveal that silt, fine sandstones and mudstones predominated on the open slope of the QNDB since, at least, the Middle Miocene.

3. Geological Setting

a) The QDNB and the evolution of the Red River Fault

The QDNB comprises a NE-trending Cenozoic Basin with an area of approximately 45,000 km^2, located in the northern part of the South China Sea (Fig. 1). The QDNB is bounded by the Hainan Island to the northwest, by the Yinggehai Basin to the west, by the Pearl River Mouth Basin to the northeast, and by the Xisha Uplift to the southeast (Fig. 1). The study area is located in the central part of the QDNB, where the basin records two main tectonic events: a rifting stage spanning the Paleocene to early Oligocene, and a post-rift stage of Early Miocene to Quaternary age (Gong and Li, 1997). Offshore, seven stratigraphic sequences can be recognized and tied to well log sections over the acoustic basement of the QDNB (Figs. 3 and 4). These sequences comprise the Yacheng Formation, the Lingshui, Sanya, Meishan, Huangliu, Yinggehai and Ledong Formations, from bottom to top (Fig. 3). These sequences are bounded by main unconformities revealed on seismic data as regional surfaces of erosional truncation: T70, T60, T50, T40, T30 and T20 (Fig. 4; Wu et al., 2009).

On a regional scale, the evolution of the QDNB is closely associated with strike-slip tectonic movements along the Red River Fault (Zhu et al., 2009). This same fault experienced sinistral strike-slip movement from Eocene to Miocene, changing to a predominant dextral regime at ~5 Ma (Allen et al., 1984; Leloup et al., 1995; Morley, 2002; Fyhn et al., 2009). In the QDNB, tectonic movements ceased at the end of Miocene, precluding a post-rift subsidence stage (Zhou et al. 1995; Sun et al. 2003). Such a change led to a significant increase in local deposition rates, which reached up to 0.7 mm/y in the Quaternary (Sun et al., 2009). An associated shelf-slope system, originated in the middle Miocene (Chen et al., 1993; Xie et al., 2006), was further developed during the post-rift stage, as recorded by the alternated deposition of thick MTDs and incision of vast systems of submarine canyons (Xie et al., 2006; Yuan et al., 2009).

ACCEPTED MANUSCRIPT

b) Margin physiography

The western border of the QDNB is coincident with the Red River Fault, a NW-SE-trending strike-slip fault active at present (Zhu et al., 2009) (Fig. 1). The study area is characterised by a relatively broad, southeast-dipping continental shelf, 200-280 km wide (Fig. 2). Major rivers comprise the main source of sediment onto the shelf, with large quantities of sediment trapped on the shelf-break (Xie et al., 2006). During sea-level lowstands, sediment by-passed the shallower zones of the margin, resulting in reduced contribution of terrigenous sediment to the outer shelf region (Xie et al., 2008).

The continental slope in the QDNB is steep (~4.5°) and incised by multiple submarine canyons and smaller submarine gullies (Figs. 5a and b). The mid- and lower slope areas are marked by the deposition of a thick wedge of the Cenozoic sediments (Figs. 1 and 4). Steeper gradients (>10°) are recorded in this region in association with widespread seafloor instability (Fig. 5b). As a result, four slide scars and thirty-two submarine canyons are presently observed in the study area (Figs. 5a and b).

4. Results

4.1 Multi-beam bathymetry

Multi-beam bathymetry provided detailed seafloor morphological data in the QDNB (Fig. 5a). Within the study area, four Holocene submarine landslides and numerous submarine canyons are identified. A detailed description of these submarine features is provided in the following paragraphs.

4.1.1 Submarine canyons

The QDNB comprises a SE-facing continental slope with a shelf break located at ~160 m water depth (Fig. 2). The shelf-break area shows several submarine canyons and slide scarps that generally strike in a NW-SE direction (Fig. 6). These canyons are essentially linear, and strike perpendicular to the slope (Fig. 5a). The heads and flanks of the canyons are carved by numerous gullies, which are relatively abundant towards the upper part of the slope, but generally absent at its base (Figs. 6a, b and d). Gullies provide direct evidence for intense erosion within the modern submarine canyons. The canyons are ~10 km to 20 km long and characterized by well-developed semicircular heads and incised amphitheatre rims (Fig. 6b). In general, the submarine canyons in the northeast part of the continental margin have more gullies than those to the southwest (Fig. 5a), which may indicate more pronounced erosion in the former region.

4.1.2 Morphology of submarine landslides

Evidence for important mass-wasting processes is observed at several locations in the QDNB (Fig. 5a). For instance, multi-beam bathymetry reveals the presence of four MTDs (A-D) on the modern seafloor (Table 1; Figs. 6a, b and c). These MTDs, and associated scars, appear to be relatively recent, as the depressions are not completely draped by hemipelagic sediment. They are all characterized by having a smooth depression upslope and a rough topographic rise downslope (Figs. 6a and c). The smooth seafloor morphology is clearly visible on the present-day seafloor, corresponding to evacuated landslide scars. In contrast, areas of rugged seafloor correspond to the depositional zones were the MTDs accumulated. The slope gradient within the evacuated scars is similar to the surrounding area (Fig. 5b).

The four Holocene MTDs are associated with U-shape headwall escarpments, which are generally 30-50 m high. Headwall escarpments of MTDs A, B and C lie at depths of 400 m to 600 m, directly connecting with canyon systems upslope (Figs. 2 and 6). MTD D has its escarpment at water depths of 1200 m to 1400 m. Evacuation zones are surrounded by escarpments, below which the accumulation zones of MTDs are clearly observed (Figs. 6a and c). Run-out distances of MTDs A to D are 34 km, 26 km, 27 km and 24 km, respectively (Table 1). In addition, MTD C has a ~50 m high escarpment, but it was not possible to identify the deposits of this slide which may probably dispersed under a thin layer of hemipelagic sediments further downslope (Fig. 6c). Estimates of the geometry and distribution of these MTDs, based on the multi-beam bathymetry data, are presented in Table 1.

4.2 Seismic data

4.2.1 Recurrent MTDs in the study area

The interpretation of recurrent MTDs followed previously-established criteria published in Frey-Martínez et al. (2005) and Bull et al. (2009), i.e. it was based on the recognition of sedimentary bodies characterized by chaotic and transparent facies bounded above, below and laterally by continuous strata (Figs. 7 and 8). The interpreted seismic data reveal several large-scale MTDs in the mid- to lower-slope regions of the QDNB (Figs. 7 and 8). These MTDs are interbedded within high-amplitude, continuous seismic reflections that likely comprise hemipelagite and turbidite

ACCEPTED MANUSCRIPT
successions similar to those documented in Gamboa et al. (2010). At their base, these MTDs are bound by basal shear surfaces marked as continuous negative reflections, generally concordant with the underlying strata (Fig. 7).

To the southwest of the study area, seven distinct Miocene to Quaternary MTDs are identified (Figs. 7 and 8). The seven MTDs were transported in a SE direction. Fig. 7 shows the stratigraphic positions of these MTDs. The spatial distribution and cross-cutting relationship were used to determine the relative timing of the MTDs. MTD 7 is the oldest in the study area (Fig. 7), and is located above the Central Canyon. Its toe region rests on the southeastern side of the Central Canyon (Fig. 7). MTDs 2 and 6 have an average thickness of ~100 m. Their upper and lower boundaries coincide with continuous, high-amplitude reflections that extend towards the southeast, beyond the limits of the seismic data set. Compared with MTD 2 and MTD 6, other MTDs have shorter run-out distances and rest on the continental slope, pinching-out towards the southeast (Figs. 7 and 8).

In the northeastern part of the QDNB, MTDs can be identified from the base of the Central Canyon to the seafloor (Fig. 9). At two-way time (TWT) depths of ~3 s, the basal shear plane of MTD 8 steeps-up dramatically to form a fontal ramp, i.e. forming a frontally confined MTD (Fig. 9). The distal limit is typically demarcated by an abrupt frontal ramp *sensu* Frey-Martínez et al. (2006). Highly deformed and discontinuous seismic reflections form in this same MTD 8 an imbricated series of thrusts in its toe region. The thrusts are formed due to local compression and comprise key kinematic indicators that constrain the movement of the MTD to a NW-SE direction.

4.2.2 Morphology and internal structure of interpreted MTDs

The detailed interpretation of 2D and 3D seismic data in the QDNB allowed the recognition of two types of MTDs based on their relative locations: a) canyon-fill MTDs, and b) open-slope MTDs (Figs. 8, 10, 11 and 12).

Several late Miocene-Quaternary submarine canyons are observed on seismic data (Fig. 10a). These canyons are filled by sediments that are characterized by chaotic to discontinuous seismic reflections of low amplitude (Fig. 10b and c). These strata are interpreted in this paper as comprising MTDs sourced from the margins of the channels and upper slope landslides. In fact, slope gradients along the submarine canyons are extremely high (Fig. 5b). Local sediment failure in canyon heads and walls are interpreted to have generated MTDs above basal channel-lag deposits, which are marked by continuous, high-amplitude reflections (Fig. 10b and c).

Open-slope MTDs are mainly observed in mid-slope regions at younger stratigraphy levels to the channels. Open-slope MTDs are characterized by presenting chaotic to discontinuous seismic reflections bounded by parallel seismic reflections above and below (Figs. 7, 8 and 9). Open-slope MTDs can comprise confined and frontally emergent MTDs sensu Frey-Martínez et al. (2006) (Fig. 8).

5. Evidence of associated slope failure and channel incision in the QNDB

Multiple geological processes have been proposed to explain the recurrence of slope instability along continental margins. Main processes include gas hydrate dissociation, tectonic oversteepening, high sedimentation rates, fluctuations in sea-level, volcanic episodes and earthquakes (Canals et al., 2004; Sultan et al., 2004a; Sultan et al., 2004b; Bryn et al., 2005; Berndt et al., 2012; Zhao et al., 2015). In this section we investigate four possible factors triggering recurrent slope failure in the QDNB: a) high sedimentation rates, b) oversteepening of the continental slope, c) tectonic reactivation and seismic activity, and d) fluctuations in sea-level. As there is no evidence of fluid flow phenomena in our study area, including the presence of free gas, pockmarks, mud diapirs and gas hydrates, we consider these latter factors as secondary triggers to slope instability in the QDNB. Such a character contrasts with areas of the South China Sea (e.g. Wang et al., 2011; Wang et al., 2014), including around the Dongsha Uplift, in which gas hydrates were systematically observed in near-seafloor sediment (Li et al., 2013; Wu et al., 2005).

Shallow sediment in the northwestern slope was chiefly sourced from the Red River into the South China Sea (Wang et al., 2013). These same authors suggest that, during the late Miocene, sediment from the Red River reached the QNDB only after the filling of the Yinggehai Basin. Resulting high sedimentation rates could have a direct impact on the building up of excess pore pressure in fine-grained sediments, which is considered as one of the principal preconditioning factors for slope failure along continental margins (Imbo et al., 2003; Sultan et al., 2004a). Recent studies yield that the central part of the QDNB experienced accelerated post-rift subsidence since the Late Miocene (10.5-0 Ma) and that sedimentation rates increased dramatically from 400 m/Myr to 800 m/Myr during this period (Zhu et al., 2011; Zhao et al., 2013). As a consequence of rapid sediment loading, recurrent slope failure events were triggered along the QDNB, as observed on the interpreted seismic data (Fig. 7b). As a result, we suggest the high sedimentation rates recorded after the Late Miocene in the study area as an important preconditioning factor for the development of the recurrent MTDs documented in this paper.

The distribution of the recurrent MTDs appears, in the QDNB, to be closely controlled by the development of an increasingly steep continental slope with time (Figs. 11 and 12). We interpret in this paper that shelf-slope systems in the QDNB formed initially during the Middle Miocene and were controlled by the reactivation of pre-existing slope-parallel faults (Figs. 1 and 11; Chen et al., 1993; Xie et al., 2008). Such an interpretation is corroborated by the seismic profiles in Figs. 11 and 12. A key observation on these seismic profiles is that the shelf margin is oversteepened and sediment mostly bypassed the shelf onto the lower slope in the form of MTDs and turbidite systems (Fig. 11). High slope gradients were later maintained by high rates of sediment supply during the Late Miocene, resulting in failure of

ACCEPTED MANUSCRIPT
the upper slope, which in turn generated large-scale mass movements further downslope (Fig. 12). At the same time, the continental slope was undercut by numerous gullies and canyons in response to widespread slope instability. Local slope undercutting by newly-formed channels and gullies created steep slopes that may later trigger further slope instability events. This widespread erosion and sediment bypass is interpreted in this paper to have resulted in the development of a highly unstable slope, generating not only large-scale MTDs but also the topographically confined MTDs that fill the larger canyons in the QDNB (Figs. 10, 11 and 12). An example of widespread sediment bypass and erosion is shown in Fig. 12, in which the slope was steepened and numerous recurrent MTDs are interpreted on the lower continental slope.

A secondary preconditioning factor in the study area is earthquake activity. Tectonic uplift in the QDNB largely ceased in the post-rift stage (15.5 Ma; Zhou et al. 1995; Xie et al. 2006), with the study area experiencing rapid subsidence events at 5.3 Ma in the west and at 10.5 Ma in the mid-east of the QDNB, respectively (Yuan et al., 2008). Nevertheless, tectonic reactivation is recorded on the continental slope throughout the study area - likely in association with movement on the Red River Fault, which changed from a sinistral strike-slip regime to dextral movement at about 5.5 Ma (Leloup et al., 1995; Zhu et al., 2009) (Fig. 1). The fault also reactivated the western part of the QDNB during the Quaternary (Schimanski and Stattegger, 2005).

High-frequency seismicity resulting from local inversion and reactivation of the Red River Fault has been recorded in the QDNB (Wei and Chung, 1995; Zhu et al., 2009; Zhu et al., 2011). In the study area, tectonic reactivation and associated earthquakes would have increased pore pressure of sediments and resulted in widespread slope instability. Moreover, along-slope faults in the northwest of the QDNB recorded a change to a dextral strike-slip regime in the Red River Fault and may have slip up to 5 km with a rate of 1-5 mm/yr since Pliocene (5.5 Ma) (Zhu et al., 2011). The reactivation of along-slope faults and related seismicity were likely responsible for the triggering of large-scale slope failures by seismic shaking and loading.

Relative sea level fluctuations in the QDNB were frequent from the late Miocene to present (Fig. 4) (Wei et al., 2001). An obvious relative sea-level drop of 100 m can be identified in the late Miocene (8.2-5.5 Ma) in the QDNB (Fig. 4). Moreover, cyclic sediment deposition associated with three cycles of main relative sea level fluctuation since 2.9 Ma was documented on the southern slope of the QDNB (Sun et al., 2011). In the QDNB, the lack of accurate age determination hampers a calibration of the emplacement of the different MTDs with relative sea level cycles. Although MTDs are considered to occur preferably during relative sea level lowstands, according to the classical sequence-stratigraphy models, recent studies carried out on passive and active continental margins have shown that, theoretically, relative sea-level fluctuations do not have an influence on slope stability and MTDs can be recognized during different (relative) sea level conditions (Laberg et al., 2002; Maslin et al., 2004; Haflidason et al., 2005; Locat et al., 2009; Twichell et al., 2009; Urlaub et al., 2013). Therefore, we conclude that the recurrence of mass-wasting in the study area was controlled by the combining action of high sedimentation rates on the shelf edge, seismic activity and oversteepening of the continental slope rather than by variations in relative sea level alone.

6. Discussion

6.1 Testing the published sequence stratigraphic models

Based on the morphology, stratigraphic distribution and different types of MTDs interpreted, we constructed a depositional model for the QDNB with the purpose of testing if the 'classical' sequence-stratigraphic models of van Wagoner et al. (1990) and Catuneanu et al. (2009) are applicable to the study area (Fig. 13). Our model provides a major tool to understand the stratigraphic importance of mass movements in steepened, bypass continental margins.

The development of recurrent MTDs in the QDNB can be synthesized in three main stages (Fig. 13). The Red River was, as it is at present, the main source of sediment to the QDNB. During the middle Miocene, the shelf-slope system in the QDNB began to develop and mass-wasting was primarily controlled by the reactivation of pre-existing along-slope faults (Fig. 13a). During the late Miocene (10.5-5.5 Ma), the QDNB entered into its subsidence stage, and sedimentation rates in the QDNB became anomalously high, reaching 550 m/Myr. This increase in sediment influx was followed by a prominent sea-level drop of ~100 m in the late Miocene, a setting that resulted in the evolution of a progradational slope (Figs. 4, 13b). This progradation is well documented by the trajectory of the shelf edge on seismic data (Fig. 11). Submarine canyons also began to develop at this time, i.e., synchronously with the triggering of small-scale MTDs. After 5.5 Ma, sedimentation rates dropped in combination with the development of a wide shelf (200-280 km) (Fig. 13c). Relatively fewer sediment was deposited on the northwestern slope of the QDNB. The sediments were mainly deposited on the outer shelf, and then progressively aggraded onto the continental margin.

During these events, slope gradients episodically (but frequently) exceeded their equilibrium gradient, triggering large gravity-controlled mass movements. The high frequency of these events resulted in the creation of a vast region of sediment by-pass on the shelf-break and upper-slope regions - a setting that contrasts with the 'classical' sequence-stratigraphic models published in van Wagoner et al. (1990) and Catuneanu et al. (2009), to cite two examples. Two features are proof of this distinct setting: a) abrupt episodes of accommodation-space generation are recorded in the shelf-edge area in association to the major episodes of instability on the continental slope (Fig. 13c); b) the filling of buried channels by MTDs implies significant erosion on the shelf edge (Figs. 10a, b and c), a setting that hints for a complete detachment between shelf and distal slope depositional systems. This setting is revealed by the diachroneity of

ACCEPTED MANUSCRIPT
most stratigraphic markers across the continental margin, with no shelf-margin progradation (nor aggradation) of sediments occurring in a uniform way along the upper slope and shelf-break regions. As a result, we propose that the reservoir potential of the QDNB, and chiefly of channel-fill deposits in the South China Sea, is closely controlled by the erosional history of the continental slope, and depends closely on the nature of the sediment (i.e. net-to-gross ratio) eroded and transported as the MTDs that fill these same channels.

Examples of regions of important continental slope bypass are known from West Iberia (Alves et al., 2003), Rockall Trough margin (Weering et al., 2003) and the Bay of Biscay (Gonthier et al., 2006). In these areas, depositional settings varied in time and space in relation to tectonic and eustatic episodes. In particular, uplifted topography in the form of seamounts are important barriers to slope-derived sediment (Alves et al., 2003), limiting sediment supply into deeper abyssal areas by forming localised sub-basins and constituting topographic barriers to slope-derived sediment. Importantly, erosional processes on the continental slope are triggered by fault-controlled subsidence of the continental rise, generating abundant turbidites, debris flows and slump deposits drilled at DSDP site 398 (Réhault and Mauffret, 1979).

Mass-wasting processes are therefore interpreted to predominate in these bypass margins, as a response to local subsidence and tectonic activity, leading to the accumulation of coarse grained debris flows, transported by submarine canyons, onto the abyssal plain.

6.2 Implications for the petroleum potential of the NE China Sea

Two significant effects on the petroleum potential of the South China Sea result from the identification of recurrent MTDs in the QDNB. The QDNB is a petroliferous basin, and many large hydrocarbon fields have been discovered in the study area (Wu et al., 2009). At least four large-scale MTDs are recognized on the modern seafloor with run-out distances of more than 20 km, denoting a significant threat to subsea installations located in the distal parts of deep-water basin is similar mass-wasting events are triggered in the future. On the other hand, the abundance of recurrent mass-wasting events in submarine canyons and open slope areas increases the risk of future hydrocarbon exploration in the study area. Net-to-gross ratios in these MTDs are closely dependent on the nature of sediment that they eroded in shelf-edge and upper-slope regions. High net-to-gross ratios have positive implications in terms of reservoir potential, but will decrease the competence of seal units eroded in shallower parts of Miocene-Quaternary slope systems to provide the strata remobilised by the recurrent MTDs. Conversely, MTDs are capable of enhancing source potential in lower slope areas by increasing burial depths for older (early Cenozoic) source intervals, a phenomenon recorded east of the QDNB in the Pearl River Mouth Basin (Zhao et al., 2015).

The second implication recognised in this paper relates to how mass-wasting processes influence the evolution of the QDNB, and of continental margins around the world. The Late Cenozoic morphology of the QDNB was strongly influenced by the emplacement of the repeated MTDs, creating an exponential profile typical of highly-eroding margins (Adams and Schlager, 2000). The occurrence of MTDs is therefore associated with important events of erosion on such exponential margins, with retrogressive failure and sediment evacuation during mass-wasting events obliterating most of the stratigraphic record on the shelf-edge and upper slope. As a result of this setting: a) strata accumulated in distal, 'base-of-slope' regions, are prone in MTDs (and relatively depleted of turbidites) on exponential margins (cf. Adams and Schlager, 2000) such as the QDNB's; b) channel-fill deposits, potentially with the higher reservoir potential, are filled with MTDs of distinct lithologies and internal organisations. In such a setting, net-to-gross ratios of failed MTDs and, particularly, the presence of megabreccias sourced from steeper proximal parts of the slope are the facies that present the most favourable potential reservoir in the QDNB, and in similar settings in the South China Sea.

In the QDNB, a case-study with implications for the entire South China Sea, relatively strike-slip tectonics was responsible for: (1) the reactivation of along-slope faults, with subsequent episodes of seafloor instability leading to the deposition of MTDs, (2) forced folding of Mesozoic-Cenozoic units, particularly along restraining bends and local pop-ups; (3) several types of fault-related traps (see Fig. 9 for an image of an uplifted horst where fault-related and stratigraphic traps are observed). This latter case is particularly important where erosion and filling of erosional paleochannels occurred, generating renewed reservoir packages at relatively shallow depths (Figs. 8 and 9). A few of the structural traps observed in the QDNB might not be related uniquely to strike-slip tectonics, a character broadening the range of potential structural traps in the study area. Particular care should also be given to differential compaction as a process capable of generating low-angle, broad folding in strata deposited below the imaged MTDs (see Alves and Cartwright, 2010). Considering the existence of a fairly homogeneous set of MTDs in the study area, to recognize the existence of structural traps in Cenozoic successions is a critical test to the existence of hydrocarbon accumulations of economic importance within continental slope basins of the South China Sea.

6.Conclusions

We have provided a detailed analysis of seafloor morphology and identified several recent submarine landslides, and shelf-incised canyons, in the central part of the QDNB, northern South China Sea. The main conclusions of this study are:

a) A significant portion of shelf-edge deposits bypassed most of the continental slope to accumulate as large MTDs

ACCEPTED MANUSCRIPT
on its lower part (i.e. in the 'basin-floor'), independently of any sea-level variations recorded during the Late Miocene-Quaternary.

b) This interpretation has implications for current sequence stratigraphic models, and sheds new light on the reservoir potential of Miocene units in the South China Sea.

c) Stratigraphically, recurrent slope instability resulted in abrupt episodes of accommodation space creation in shelf-edge regions.

d) The setting observed in the QDNB records a complete detachment between shelf and distal slope depositional systems, with most stratigraphic markers on 3D seismic data being markedly diachronous across the continental margin.

e) As MTDs also comprise the bulk of channel-fill deposits in large submarine canyons. Reservoir potential in the South China Sea is closely dependent on the nature (i.e. net-to-gross ratios) of sediment eroded and transported by discrete MTDs.

Acknowledgments

We acknowledge China National Offshore Oil Corporation for their permissions to release the seismic data. This research was supported by National Basic Research Program of China (No. 2015CB251201) and Key Project of Natural Science Foundation of China Foundation (No. 91228208 and No. Sidsse-201403). The paper benefited from the comments of Makoto Ito and two helpful, but anonymous, reviewers whose constructive suggestions greatly improved this manuscript.

References

Adams, E.W., Schlager, W., 2000. Basic Types of Submarine Curvature: J. Sediment. Res. 70, 814-828.

Allen, C.R., Gillespie, A.R., Han, Y., Sieh, K.E., Zhang, B., Zhu, C., 1984. Red River and associated faults, Yunnan Province, China: Quaternary geology, slip rates and seismic hazard. Geol. Soc. Amer. Bull. 95, 686-700.

Alves, T.M., Cartwright, J.A., 2010. The effect of mass-transport deposits on the younger slope morphology, offshore Brazil. Mar. Pet. Geol. 27, 2027-2036.

Alves, T.M., Kurtev, K., Moore, G.F., Strasser, M., 2014. Assessing the internal character, reservoir potential, and seal competence of mass-transport deposits using seismic texture: A geophysical and petrophysical approach. AAPG Bull. 98, 793-824.

Alves, T.M., Manuppella, G., Gawthorpe, R.L., Hunt, D.W., Monteiro, J.H., 2003. The depositional evolution of diapir- and fault-bounded rift basins: examples from the Lusitanian Basin of West Iberia. Sediment. Geology. 162, 273-303.

Berndt, C., Costa, S., Canals, M., Camerlenghi, A., de Mol, B., Saunders, M., 2012. Repeated slope failure linked to fluid migration: The Ana submarine landslide complex, Eivissa Channel, Western Mediterranean Sea. Earth Planet. Sc. Lett. 319-320, 65-74.

Bryn, P., Berg, K., Forsberg, C.F., Solheim, A., Kvalstad, T.J., 2005. Explaining the Storegga Slide. Mar. Pet. Geol. 22, 11-19.

Bull, S., Cartwright, J., Huuse, M., 2009. A review of kinematic indicators from mass-transport complexes using 3D seismic data. Mar. Pet. Geol. 26, 1132-1151.

Canals, M., Lastras, G., Urgeles, R., Casamor, J.L., Mienert, J., Cattaneo, A., De Batist, M., Haflidason, H., Imbo, Y., Laberg, J.S., Locat, J., Long, D., Longva, O., Masson, D.G., Sultan, N., Trincardi, F., Bryn, P., 2004. Slope failure dynamics and impacts from seafloor and shallow sub-seafloor geophysical data: case studies from the COSTA project. Mar. Geol. 213, 9-72.

Catuneanu, O., Abreu, V., Bhattacharya, J.P., Blum, M.D., Dalrymple, R.W., Eriksson, P.G., Fielding, C.R., Fisher, W.L., Galloway, W.E., Gibling, M.R., Giles, K.A., Holbrook, J.M., Jordan, R., Kendall, C.G.S.C., Macurda, B., Martinsen, O.J., Miall, A.D., Neal, J.E., Nummedal, D., Pomar, L., Posamentier, H.W., Pratt, B.R., Sarg, J.F., Shanley, K.W., Steel, R.J., Strasser, A., Tucker, M.E., Winker, C., 2009. Towards the standardization of sequence stratigraphy. Earth-Sci. Rev. 92, 1-33.

Chen, P. H., Chen, Z.Y., Zhang, Q.M., 1993. Sequence stratigraphy and continental margin development of the northwestern shelf of the South China Sea. AAPG Bull. 77 (5), 842-862.

Frey-Martínez, J., Cartwright, J., James, D., 2006. Frontally confined versus frontally emergent submarine landslides: A 3D seismic characterisation. Mar. Pet. Geol. 23, 585-604.

ACCEPTED MANUSCRIPT

Frey-Martínez, J., Cartwright, J., Hall, B., 2005. 3D seismic interpretation of slump complexes: examples from the continental margin of Israel. Basin Res. 17, 83-108.

Fyhn, M.B.W., Boldreel, L.O., Nielsen, L.H., 2009. Geological development of the Central and South Vietnamese margin: Implications for the establishment of the South China Sea, Indochinese escape tectonics and Cenozoic volcanism. Tectonophysics 478, 184-214.

Galloway, W.E., and Dutton, S.P., 1979, Seismic stratigraphic analysis of intracratonic basin sandstone reservoirs, in Pennsylvanian sandstones of the Mid-Continent: Tulsa Geol. Soc. Spec. Publication No. 1, 65–81.

Gamboa, D., Alves, T., Cartwright, J., Terrinha, P., 2010. MTD distribution on a 'passive' continental margin: The Espírito Santo Basin (SE Brazil) during the Palaeogene. Mar. Pet. Geol. 27, 1311-1324.

Gee, M.J.R., Gawthorpe, R.L., Friedmann, S.J., 2006. Triggering and Evolution of a Giant Submarine Landslide, Offshore Angola, Revealed by 3D Seismic Stratigraphy and Geomorphology. J. Sediment. Res. 76, 9-19.

Gong, Z.S., Li, S.T., 1997. Continental margin basin analysis and hydrocarbon accumulation of the northern South China Sea. Science Press, Beijing, 193–256.

Gonthier E., Cirac P., Faugeres J., Gaudin M., Cremer M., Bourillet J., 2006. Instabilities and deformation in the sedimentary cover on the upper slope of the southern Aquitaine continental margin, north of the Capbreton canyon (Bay of Biscay). Sci. Mar. 70, 89-100.

Haflidason, H., Lien, R., Sejrup, H.P., Forsberg, C.F., Bryn, P., 2005. The dating and morphometry of the Storegga Slide. Mar. Pet. Geol. 22, 123-136.

He, J.X., Xia, B., Sun, D.S., Zhang, S.L., Liu, B.M., 2006. Hydrocarbon accumulation, migration and play targets in the Qiongdongnan Basin, South China Sea. Petro. Explor. and Develop. 33, 53–58.

Hunt, D., Gawthorpe, R.L., 2000. Sedimentary Responses to Forced Regressions. J. Geol. Soc. London, Special Publications, 172, 1-383.

Imbo, Y., De Batist, M., Canals, M., Prieto, M.J., Baraza, J., 2003. The Gebra Slide: a submarine slide on the Trinity Peninsula Margin, Antarctica. Mar. Geol. 193, 235-252.

Krastel, S., Wynn, R., Georgiopoulou, A., Geersen, J., Henrich, R., Meyer, M., Schwenk, T., 2012. Large-Scale Mass Wasting on the Northwest African Continental Margin: Some General Implications for Mass Wasting on Passive Continental Margins, in: Yamada, Y., Kawamura, K., Ikehara, K., Ogawa, Y., Urgeles, R., Mosher, D., Chaytor, J., Strasser, M. (Eds.), Submarine Mass Movements and Their Consequences. Springer Netherlands, 189-199.

Krastel, S., Wynn, R.B., Hanebuth, T.J.J., Henrich, R., Holz, C., Meggers, H., Kuhlmann, H., Georgiopoulou, A., Schulz, H.D., 2006. Mapping of seabed morphology and shallow sediment structure of the Mauritania continental margin, Northwest Africa: some implications for geohazard potential. Norw. J. Geol. 86, 163-176.

Laberg, J., Vorren, T., Mienert, J., Bryn, P., Lien, R., 2002. The Trænadjupet Slide: a large slope failure affecting the continental margin of Norway 4,000 years ago. Geo-Mar. Lett. 22, 19-24.

Lee, S., Stow, D.V., 2007. Laterally contiguous, concave-up basal shear surfaces of submarine landslide deposits (Miocene), southern Cyprus: differential movement of sub-blocks within a single submarine landslide lobe. Geosci. J. 11, 315-321.

Leloup, P.H., Lacassin, R., Tapponnier, P., Schärer, U., Zhong, D., Liu, X., Zhang, L., Ji, S., Trinh, P.T., 1995. The Ailao Shan-Red River shear zone (Yunnan, China), Tertiary transform boundary of Indochina. Tectonophysics 251, 3-84.

Li, L., Lei, X., Zhang, X., Sha, Z., 2013. Gas hydrate and associated free gas in the Dongsha Area of northern South China Sea. Mar. Pet. Geol. 39, 92-101.

Li, W., Wu, S., Völker, D., Zhao, F., Mi, L., Kopf, A., 2014. Morphology, seismic characterization and sediment dynamics of the Baiyun Slide Complex on the northern South China Sea margin. J. Geol. Soc. London 171, 865-877.

Li, X., Fairweather, L., Wu, S., Ren, J., Zhang, H., Quan, X., Jiang, T., Zhang, C., Su, M., He, Y., Wang, D., 2013. Morphology, sedimentary features and evolution of a large palaeo submarine canyon in Qiongdongnan basin, Northern South China Sea. J. Asian Earth Sci. 62, 685-696.

Locat, J., Lee, H.J., 2002. Submarine landslides: advances and challenges. Can. Geotech. J. 39, 193-212.

Locat, J., Lee, H., ten Brink, U.S., Twichell, D., Geist, E., Sansoucy, M., 2009. Geomorphology, stability and mobility of the

ACCEPTED MANUSCRIPT

Currituck slide. Mar. Geol. 264, 28-40.

Maslin, M., Owen, M., Day, S., Long, D., 2004. Linking continental-slope failures and climate change: Testing the clathrate gun hypothesis. Geology 32, 53.

Masson, D.G., Harbitz, C.B., Wynn, R.B., Pedersen, G., Lovholt, F., 2006. Submarine landslides: processes, triggers and hazard prediction. Philos. Trans. R. Soc. Lond., A 364, 2009-2039.

Migeon, S., Cattaneo, A., Hassoun, V., Larroque, C., Corradi, N., Fanucci, F., Dano, A., Mercier de Lepinay, B., Sage, F., Gorini, C., 2011. Morphology, distribution and origin of recent submarine landslides of the Ligurian Margin (North-western Mediterranean): some insights into geohazard assessment. Mar. Geophys. Res. 32, 225-243.

Morley, C.K., 2002. A tectonic model for the Tertiary evolution of strike–slip faults and rift basins in SE Asia. Tectonophysics 347, 189-215.

Moscardelli, L., Wood, L., 2008. New classification system for mass transport complexes in offshore Trinidad. Basin Res. 20, 73-98.

Moscardelli, L., Wood, L., Mann, P., 2006. Mass-transport complexes and associated processes in the offshore area of Trinidad and Venezuela. AAPG Bull. 90, 1059-1088.

Posamentier, H.W., Kolla, V., 2003. Seismic Geomorphology and Stratigraphy of Depositional Elements in Deep-Water Settings. Journal of Sediment. Res. 73, 367-388.

Réhault, J.P. and Mauffret, A., 1979. Relationship between tectonics and sedimentation around the northwestern Iberian margin. In Sibuet, J. C , Ryan, W. B. F , et al., Init. Repts. DSDP, 47, Pt. 2: Washington (U.S. Govt. Printing Office), 663-682.

Schimanski, A., Stattegger, K., 2005. Deglacial and Holocene evolution of the Vietnam shelf: stratigraphy, sediments and sea-level change. Mar. Geol. 214, 365-387.

Yuan, S., Wu, S., Thomas, L., Yao, G., Lv F., Cao, F., Wang, H., Li, L., 2009. Fine-grained Pleistocene deepwater turbidite channel system on the slope of Qiongdongnan Basin, northern South China Sea. Mar. Pet. Geol. 26, 1441-1451.

Sultan, N., Cochonat, P., Canals, M., Cattaneo, A., Dennielou, B., Haflidason, H., Laberg, J.S., Long, D., Mienert, J., Trincardi, F., Urgeles, R., Vorren, T.O., Wilson, C., 2004a. Triggering mechanisms of slope instability processes and sediment failures on continental margins: a geotechnical approach. Mar. Geol. 213, 291-321.

Sultan, N., Cochonat, P., Foucher, J.P., Mienert, J., 2004b. Effect of gas hydrates melting on seafloor slope instability. Mar. Geol. 213, 379-401.

Sun, Q., Wu, S., Lüdmann, T., Wang, B., Yang, T., 2011. Geophysical evidence for cyclic sediment deposition on the southern slope of Qiongdongnan Basin, South China Sea. Mar. Geophys. Res. 32, 415-428.

Sun, Q., Wu, S., Yao, G., Lü, F., 2009. Characteristics and formation mechanism of polygonal faults in Qiongdongnan Basin, northern South China Sea. J. Earth Sci. 20, 180-192.

Sun, Z., Zhou, D., Zhong, Z., Zeng, Z., Wu, S., 2003. Experimental evidence for the dynamics of the formation of the Yinggehai basin, NW South China Sea. Tectonophysics 372, 41-58.

Twichell, D.C., Chaytor, J.D., ten Brink, U.S., Buczkowski, B., 2009. Morphology of late Quaternary submarine landslides along the U.S. Atlantic continental margin. Mar. Geol. 264, 4-15.

Urlaub, M., Talling, P.J., Masson, D.G., 2013. Timing and frequency of large submarine landslides: implications for understanding triggers and future geohazard. Quaternary Sci. Rev. 72, 63-82.

van Wagoner, et al, 1990, “Siliciclastic Sequence. Stratigraphy in Well Logs, Cores, and Outcrops”,. AAPG Methods in Exploration Series No. 7.

Völker, D., Scholz, F., Geersen, J., 2011. Analysis of submarine landsliding in the rupture area of the 27 February 2010 Maule earthquake, Central Chile. Mar. Geol. 288, 79-89.

Wang, D., Wu, S., Qin, Z., Spence, G., Lü, F., 2013. Seismic characteristics of the Huaguang mass transport deposits in the Qiongdongnan Basin, South China Sea: Implications for regional tectonic activity. Mar. Geol. 346, 165-182.

Wang, X., Hutchinson, D.R., Wu, S., Yang, S., Guo, Y., 2011. Elevated gas hydrate saturation within silt and silty clay sediments in the Shenhu area, South China Sea. J. Geophys. Res. 116 (B05102), 1-18.

Wang, X., Lee, M., Collett, T., Yang, S., Guo, Y., Wu, S., 2014. Gas hydrate identified in sand-rich inferred sedimentary section using downhole logging and seismic data in Shenhu area, South China Sea. Mar. Pet. Geol. 51, 298-306.

ACCEPTED MANUSCRIPT

Wei, B., Chung, W., 1995. Strike-slip faulting on the northern margin of the South China Sea: evidence from two earthquakes offshore of Hainan Island, China, in December 1969. Tectonophysics 241, 55-66.

Wei, K., Cui, H., Ye, S., Li, D., Liu, T., Liang, J., Yang, G., Wu, L., Zhou, X., Hao, Y., 2001. High-precision sequence stratigraphy in Qiongdongnan Basin. J. China Uni. Geoscie. 26, 59-66 (in Chinese with English abstract).

Weimer, P., 1989. Sequence stratigraphy of the Mississippi fan (Plio-Pleistocene), Gulf of Mexico. Geo-Mar. Lett. 9, 185-272.

Wu, S., Qin, Z., Wang, D., Peng, X., Wang, Z., Yao, G., 2011. Analysis on Seismic Characteristics and Triggering Mechanisms of Mass Transport Deposits on the Northern Slope of the South China Sea. Chin. J. Geophys. 54, 1056-1068.

Wu, S., Yang, Z., Wang, D., Lü, F., Lüdmann, T., Fulthorpe, C., Wang, B., 2014. Architecture, development and geological control of the Xisha carbonate platforms, northwestern South China Sea. Mar. Geol. 350, 71-83.

Wu, S., Yuan, S., Zhang, G., Ma, Y., Mi, L., Xu, N., 2009. Seismic characteristics of a reef carbonate reservoir and implications for hydrocarbon exploration in deepwater of the Qiongdongnan Basin, northern South China Sea. Mar. Pet. Geol. 26, 817-823.

Wu, S., Zhang, G., Huang, Y., Liang, J., Wong, H.K., 2005. Gas hydrate occurrence on the continental slope of the northern South China Sea. Mar. Pet. Geol. 22, 403-412.

Xie, X., Müller, R.D., Li, S., Gong, Z., Steinberger, B., 2006. Origin of anomalous subsidence along the Northern South China Sea margin and its relationship to dynamic topography. Mar. Pet. Geol. 23, 745-765.

Xie, X., Müller, R.D., Ren, J., Jiang, T., Zhang, C., 2008. Stratigraphic architecture and evolution of the continental slope system in offshore Hainan, northern South China Sea. Mar. Geol. 247, 129-144.

Yuan, S., Lü, F., Wu, S., Yao, G., Ma, Y., Fu, Y., 2009. Seismic stratigraphy of the Qiongdongnan deep sea channel system, northwest South China Sea. Chin. J. Oceanol. Limn. 27, 250-259.

Yuan, Y., Yang, S., Hu, S., He, L., 2008. Tectonic subsidence of Qiongdongnan Basin and its main control factors. Chin. J. Geophys. 51 (2), 248-255.

Zhao, F., Alves, T.M., Li, W., Wu, S., Recurrent slope failure enhancing source rock burial depth and seal unit competence in the Pearl River Mouth Basin, offshore South China Sea. Tectonophysics (in press).

Zhao, Z., Sun, Z., Wang, Z., Sun, Z., Liu, J., Wang, Z., Sun, L., 2013. The dynamic mechanism of post-rift accelerated subsidence in Qiongdongnan Basin, northern South China Sea. Mar. Geophys. Res. 34, 295-308.

Zhou, D., Ru, K., Chen, H.., 1995. Kinematics of Cenozoic extension on the South China Sea continental margin and its implications for the tectonic evolution of the region. Tectonophysics 251, 161-177.

Zhu, M., Graham, S., McHargue, T., 2009. The Red River Fault zone in the Yinggehai Basin, South China Sea. Tectonophysics 476, 397-417.

Zhu, M., Mchargue, T., Graham, S.A., 2011. 3-D seismic-reflection characterization of submarine slides on a Pliocene siliciclastic continental slope and its implications for tectonics, sediment supply, and climate change, South China Sea. In: Shipp, C., Weimer, P., and Posamentier, H. (Eds.), Submarine slope systems. SEPM Special Publications, 96, 111-126.

Figure Captions

Fig. 1 Combined bathymetric and topographic map showing the locations of sedimentary basins in the northern part of the South China Sea. The study area (black box) is located in the central part of the QDNB. The location of major structures and geological features (e.g. Red River Fault, Central Canyon and slope-parallel faults) are taken from Xie et al. (2008) and Gong et al. (2011).

Fig. 2 Depth contour map showing the submarine channels, the Changchang depression and the Xisha Horst (see Fig. 1 for location). The blue box represents the location of Fig. 5. The red boxes show the location of the two 3D seismic volumes interpreted in this paper. White solid lines highlight the location of 2D seismic profiles shown in this paper. The red dot shows the location of Well LS33-1.

Fig. 3 Lithological column highlighting main sequences and relative sea-level variations in the QDNB during the Paleogene-Quaternary (modified after Wu et al., 2009). Sea level curves for the QDNB were adopted from Wei et al. (2001). The eustatic sea-level curve is taken from Haq et al. (1987).

ACCEPTED MANUSCRIPT

Fig. 4 (a) 2D seismic profile across the Central Canyon (see Fig. 2 for location). (b) Corresponding interpretation showing seven seismic sequences. The ages of seismic surfaces are based on stratigraphic data from Well LS33-1 and on data from Wu et al. (2014).

Fig. 5 (a) Bathymetric map highlighting the presence of thirty-two (32) submarine channels and four (4) MTDs in the QDNB. Blue rectangles show the locations of Figures 6a-6d. (b) Seabed slope angle map highlighting the high slope angles observed in submarine channels and slide scarps.

Fig. 6 Seafloor morphology of four distinct areas of the QDNB, showing four MTDs with evacuated headwall scars and accumulated sediments in the toe regions of the slope. Incised submarine channels in the northeast of the continental margin (Fig. 6d) show more slope gullies than those in the southwest (Fig. 6b) (see Fig. 5a for location).

Fig. 7 (a) 2D dip-oriented seismic section from the western part of the study area (see Fig. 2 for location). (b) Interpreted seismic section, showing the stratigraphic context of the seven MTDs interpreted in this paper. The MTDs are characterized by chaotic amplitude reflections, in contrast to adjacent strata separating them. The seven MTDs are younger than 5.5 Ma (T30).

Fig. 8 (a) Along-strike oriented seismic section highlighting the recurrent MTDs interpreted in the study area (see Fig. 2 for location). (b) Interpreted seismic section showing stratigraphic context of the recurrent MTDs. MTD 2 and MTD 6 are also recognized in Figure 7.

Fig. 9 (a) Seismic section across the Central Canyon. (b) Interpreted seismic section showing recurrent MTDs developed within and above the Central Canyon. Note the presence of an uplifted horst leading to forced-folding of strata to the SE of the interpreted profile. The seismic section also reveals a frontal ramp and several well-developed thrusts in MTD 8.

Fig. 10 (a) 2D seismic section extracted from the interpreted 3D seismic volume (see Fig. 2 for location) showing the seismic expression of recurrent MTDs accumulated within Late Pliocene-Quaternary submarine canyons. (b) Vertically-stacked submarine canyons were mostly filled by MTDs, some of which can be sandy in nature. (c) Within the most recent canyons, there is evidence of small-scale MTDs transported from the flank of the canyons.

Fig. 11 2D seismic profile through the shelf-slope of the QDNB (see Fig. 2 for location). Slope-parallel faults related to tectonic uplift penetrated the younger strata, at places reaching the seafloor. Chaotic facies reflecting the presence of MTDs are distributed within the canyons and open slope area. A steepening shelf-margin after 5.5 Ma (T30) suggests decreased sediment supply and increased mass movements in the Late Cenozoic-Quaternary.

Fig. 12 2D seismic line (see location in Fig. 2) across the shelf-slope of the QDNB showing a oversteepened slope, canyon-filled MTDs and open-slope MTDs that were accumulated in lower-slope areas.

Fig. 13 Depositional model for the development of recurrent MTDs in the QDNB and on by-pass margins such as those referred to in the discussion. (a) Initiation of the shelf-slope system in the QDNB during the Middle Miocene. Canyon-fill MTDs developed accompanied the formation of submarine canyons. (b) During the Late Miocene, open-slope MTDs began to develop due to the increasingly high sedimentation rates and reactivation of pre-existing slope-parallel faults. (c) After 5.5 Ma (T30), sedimentation rates decreased and the continental shelf became wider, leading to oversteepening of the shelf margin. Most of the sediments were deposited on the outer shelf. The shelf margin shows a nearly vertical stacking pattern. Modern MTDs observed on the seafloor indicate the continental margin in the QDNB to be still dominated by MTDs.

ACCEPTED MANUSCRIPT

Table 1 Estimated length, width, average thickness, volume and maximum run-out distance of MTD A to D (see Fig. 6 for location).

ACCEPTED MANUSCRIPT

ACCEPTED MANUSCRIPT

MTD	Length (km)	Width (km)	Average thickness (m)	Volume (km^3)	Max run-out (km)
MTD A	21	3.8	20	1.596	36
MTD B	14	6.5	20	1.82	26
MTD C	19	7	20	2.66	27
MTD D	20	3.6	20	1.44	24

ACCEPTED MANUSCRIPT

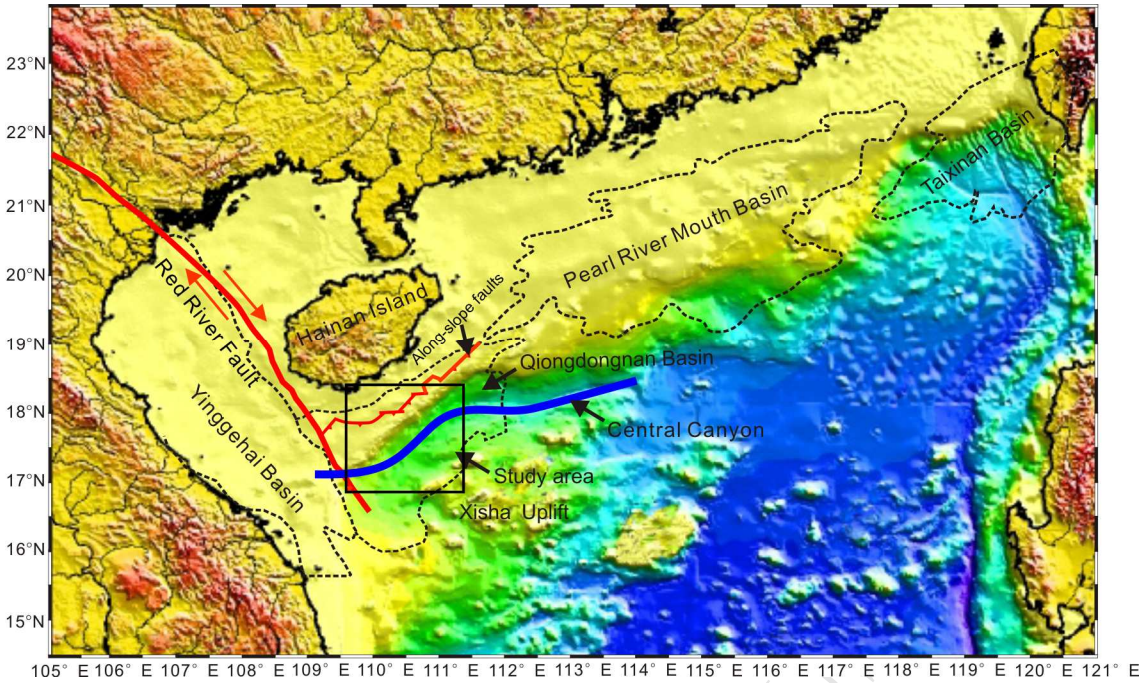

ACCEPTED MANUSCRIPT

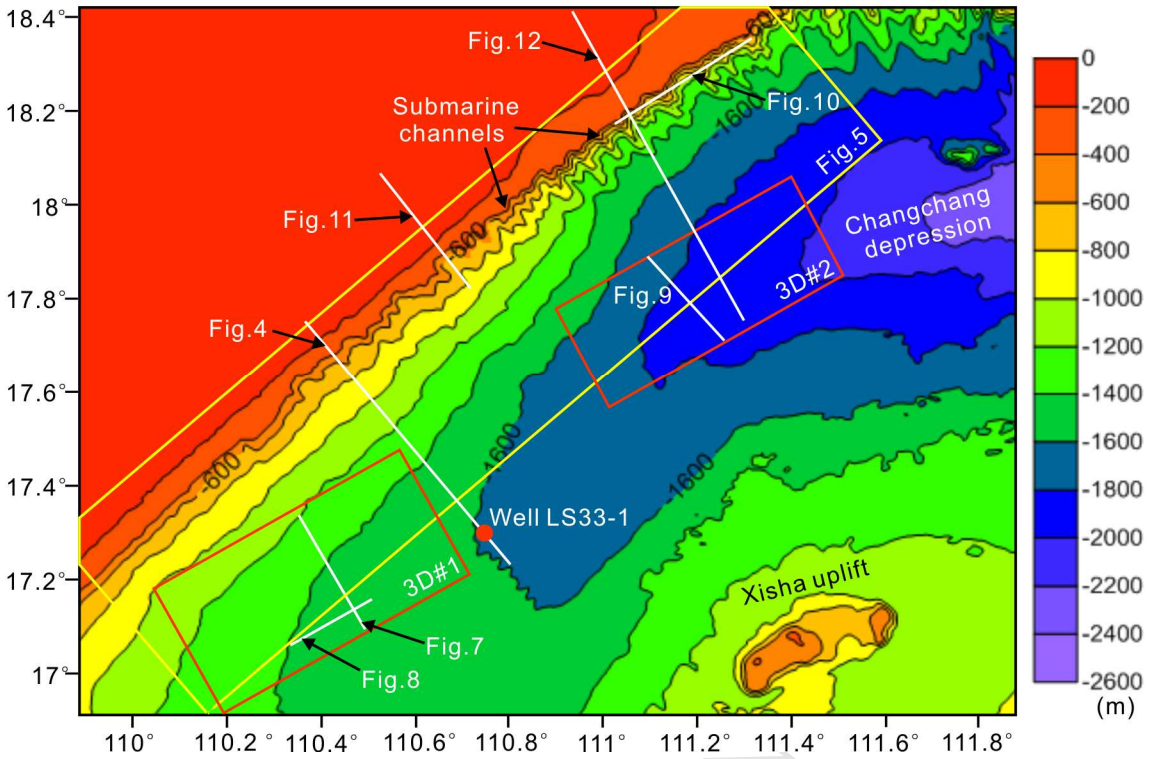

ACCEPTED MANUSCRIPT

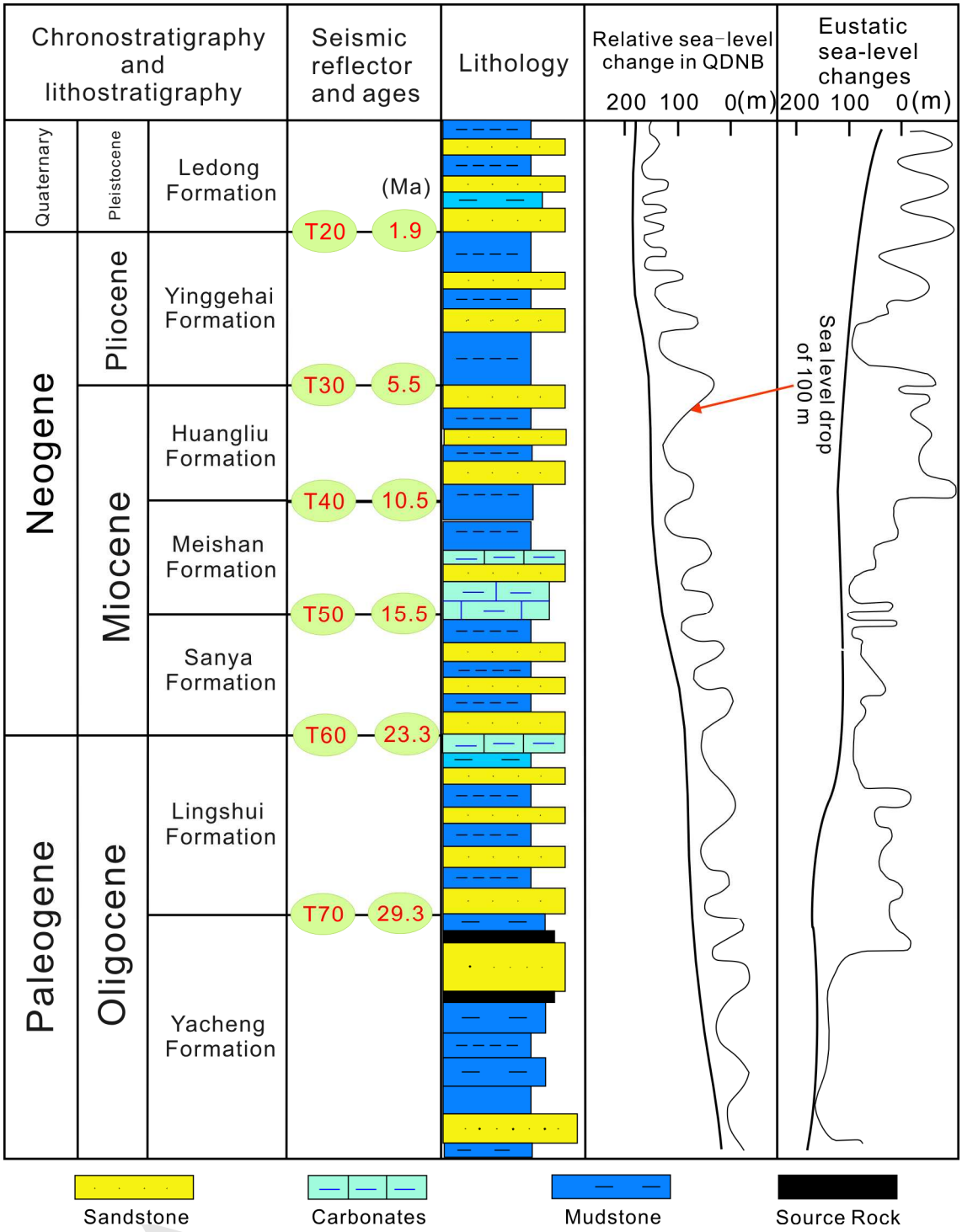
Chronostratigraphy and lithostratigraphy
Seismic reflector and ages
Lithology
Relative sea-level change in QDNB
200 100 0(m)
Eustatic sea-level changes
200 100 0(m)
Quaternary
Pleistocene
Ledong Formation
(Ma)
T20
1.9
Neogene
Pliocene
Yinggehai Formation
T30
5.5
Miocene
Huangliu Formation
T40
10.5
Meishan Formation
T50
15.5
Sanya Formation
T60
23.3
Paleogene
Oligocene
Lingshui Formation
T70
29.3
Yacheng Formation
Sea level drop of 100 m
Sandstone
Carbonates
Mudstone
Source Rock

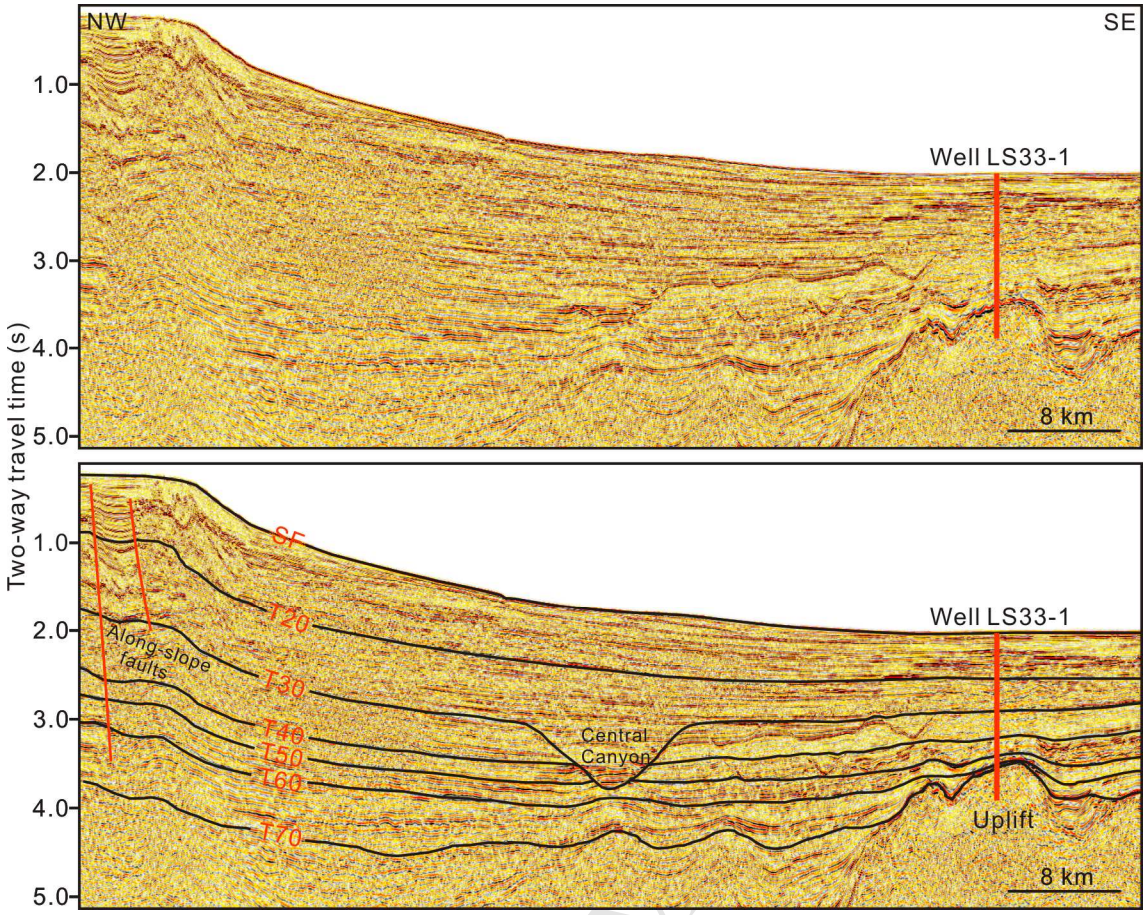

ACCEPTED MANUSCRIPT

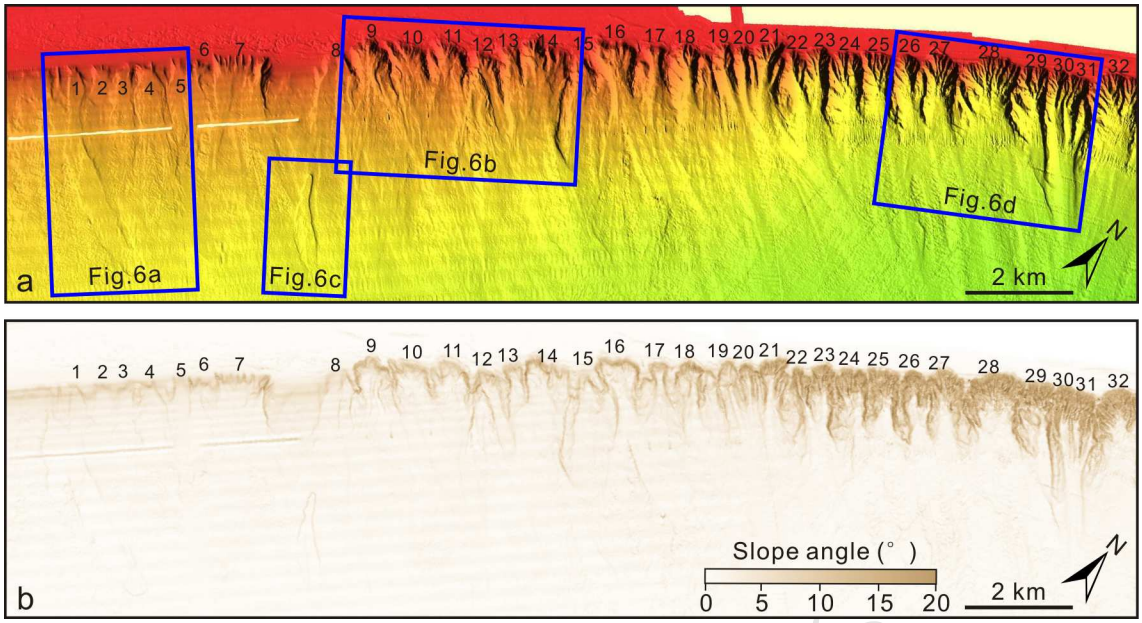

ACCEPTED MANUSCRIPT

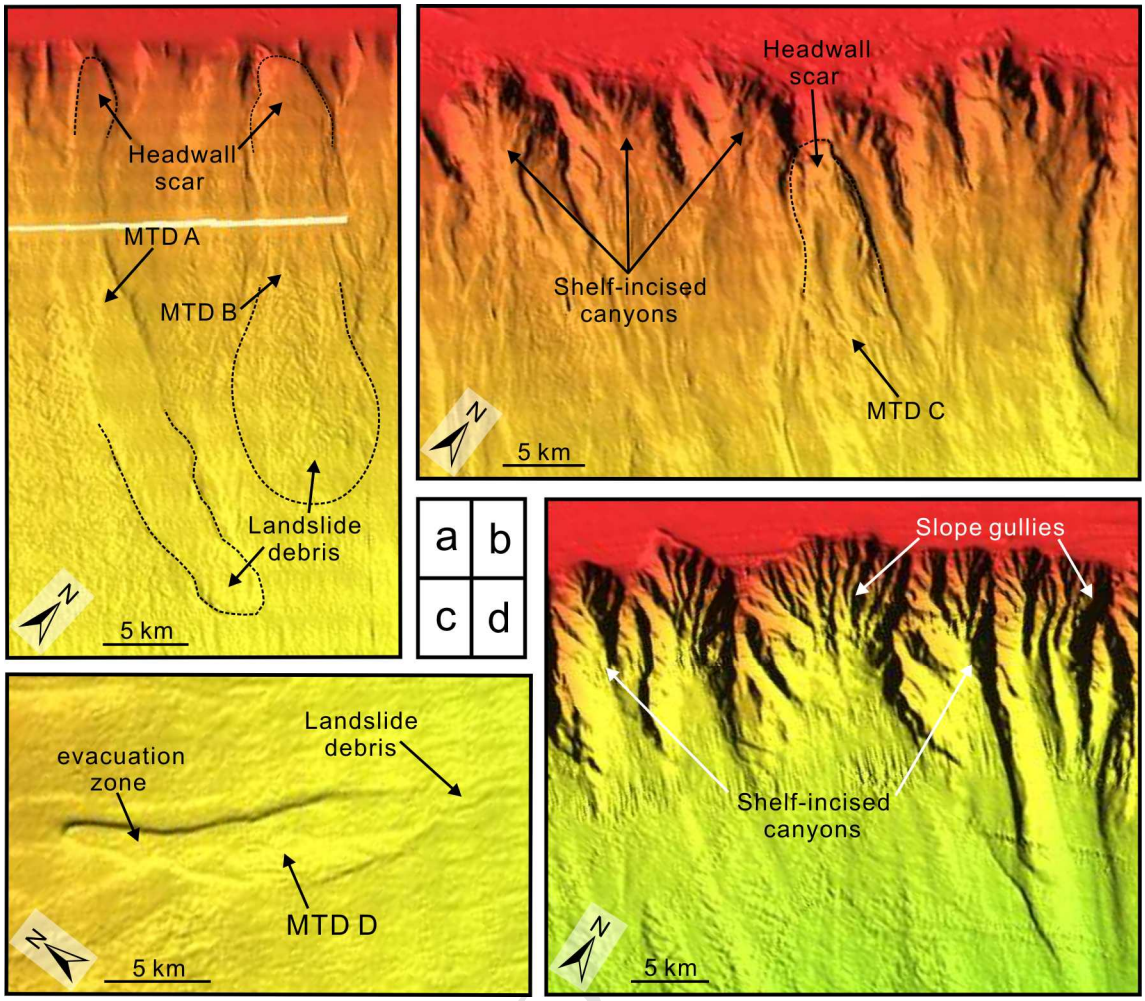
Headwall scar
MTD A
MTD B
Landslide debris
5 km
Headwall scar
Shelf-incised canyons
MTD C
5 km
a
b
c
d
Slope gullies
Shelf-incised canyons
5 km
Landslide debris
evacuation zone
MTD D
5 km

ACCEPTED

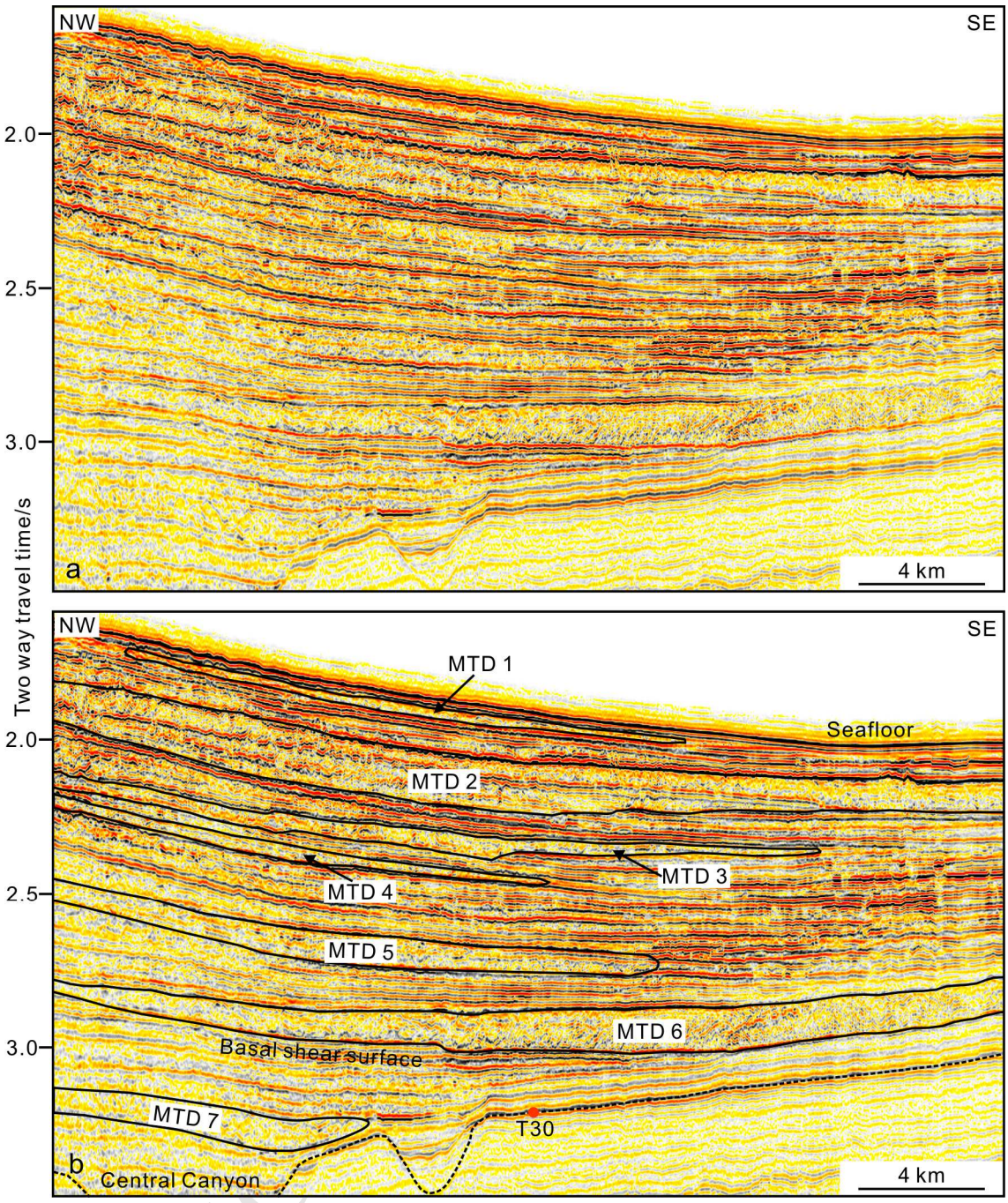
NW
SE
2.0
2.5
3.0
Two way travel time/s
a
4 km
NW
SE
MTD 1
Seafloor
MTD 2
MTD 3
MTD 4
MTD 5
MTD 6
Basal shear surface
MTD 7
T30
b
Central Canyon
4 km

ACCEPTED MANUSCRIPT

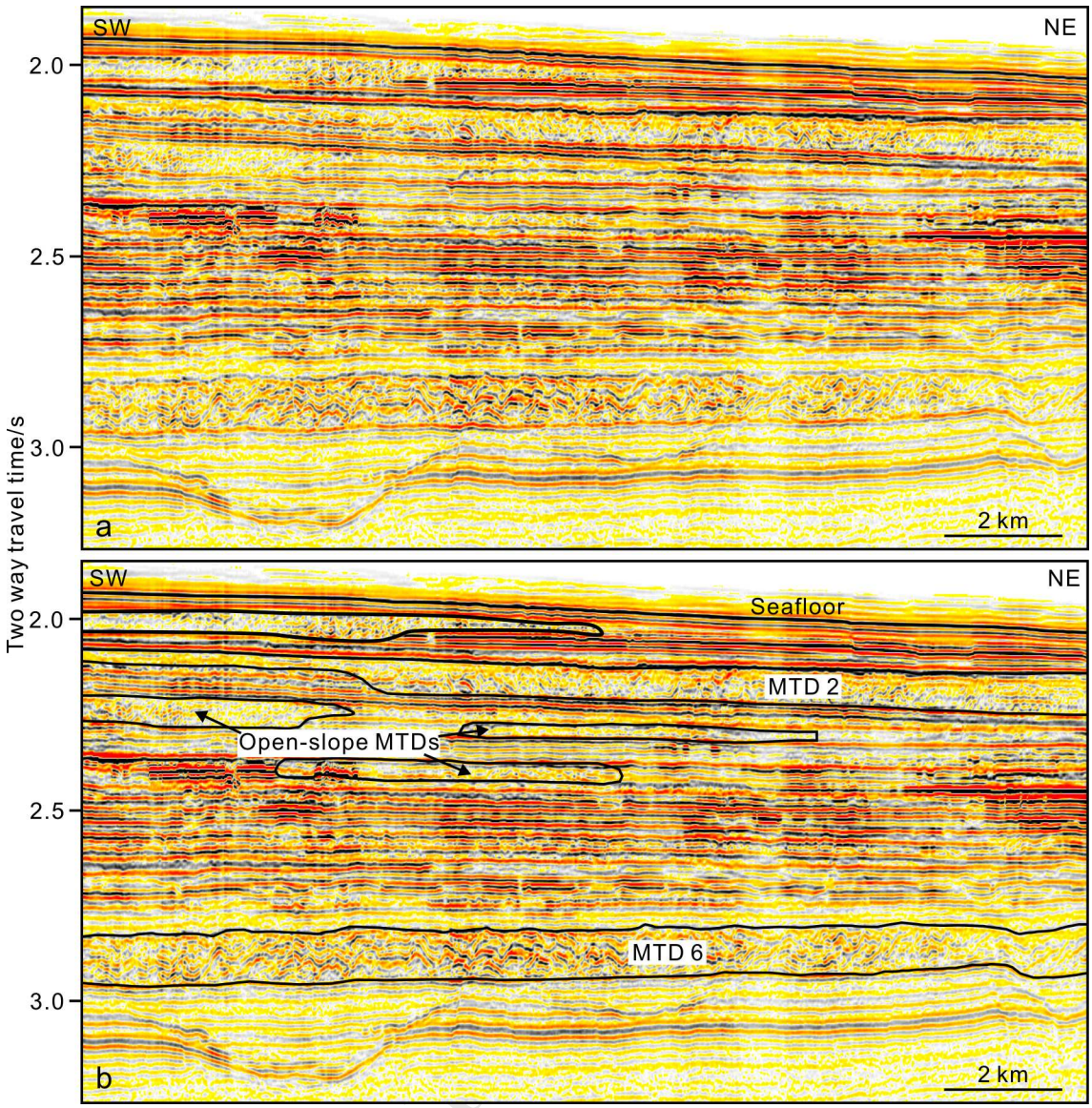

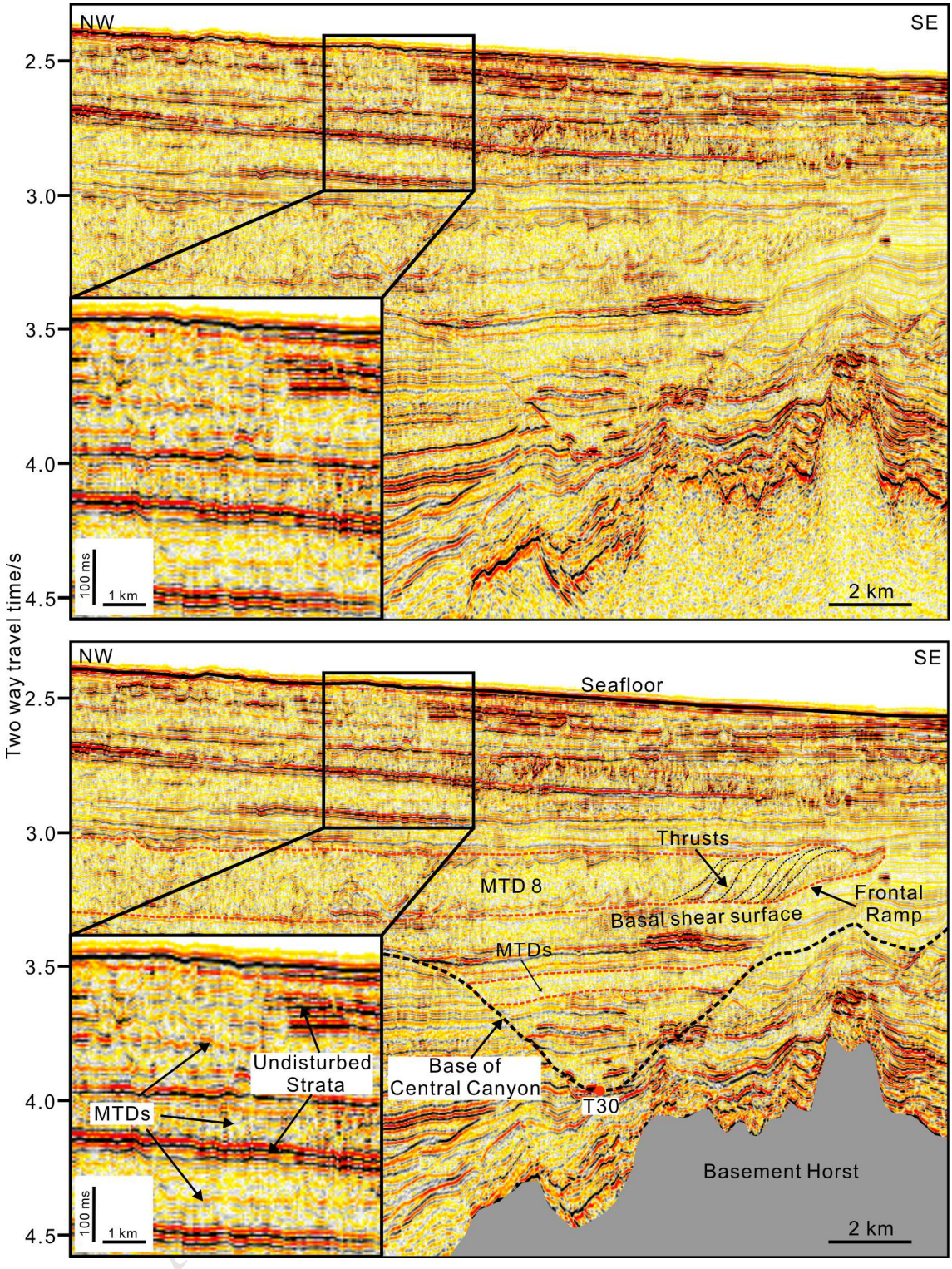
NW
SE
2.5
3.0
3.5
4.0
4.5
Two way travel time/s
100 ms
1 km
2 km
Seafloor
Thrusts
MTD 8
Basal shear surface
Frontal Ramp
MTDs
Undisturbed Strata
Base of Central Canyon
T30
Basement Horst

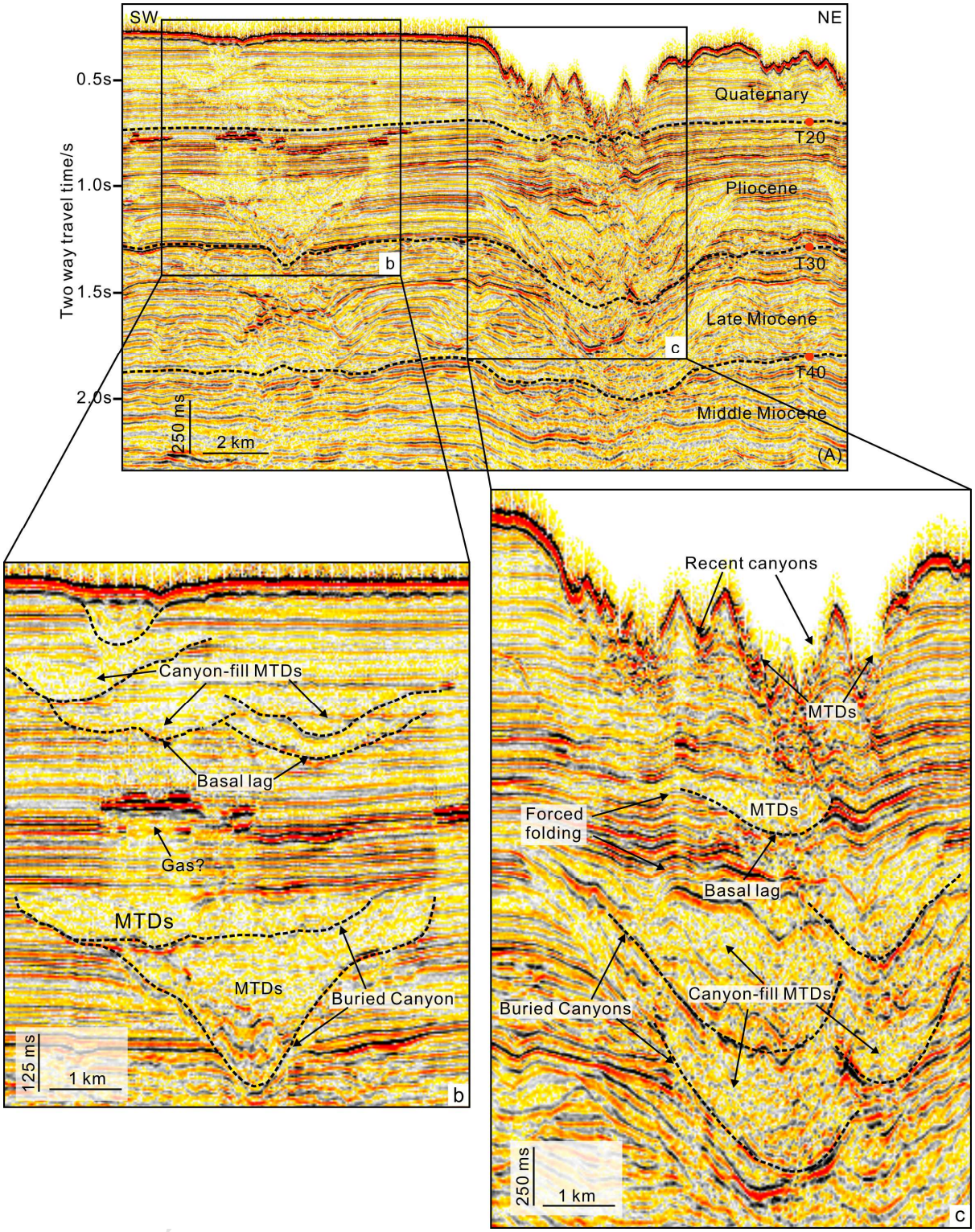
SW
NE
0.5s
1.0s
1.5s
2.0s
Two way travel time/s
Quaternary
T20
Pliocene
T30
Late Miocene
T40
Middle Miocene
b
c
250 ms
2 km
(A)
Canyon-fill MTDs
Basal lag
Gas?
MTDs
MTDs
Buried Canyon
125 ms
1 km
b
Recent canyons
MTDs
Forced folding
MTDs
Basal lag
Buried Canyons
Canyon-fill MTDs
250 ms
1 km
c

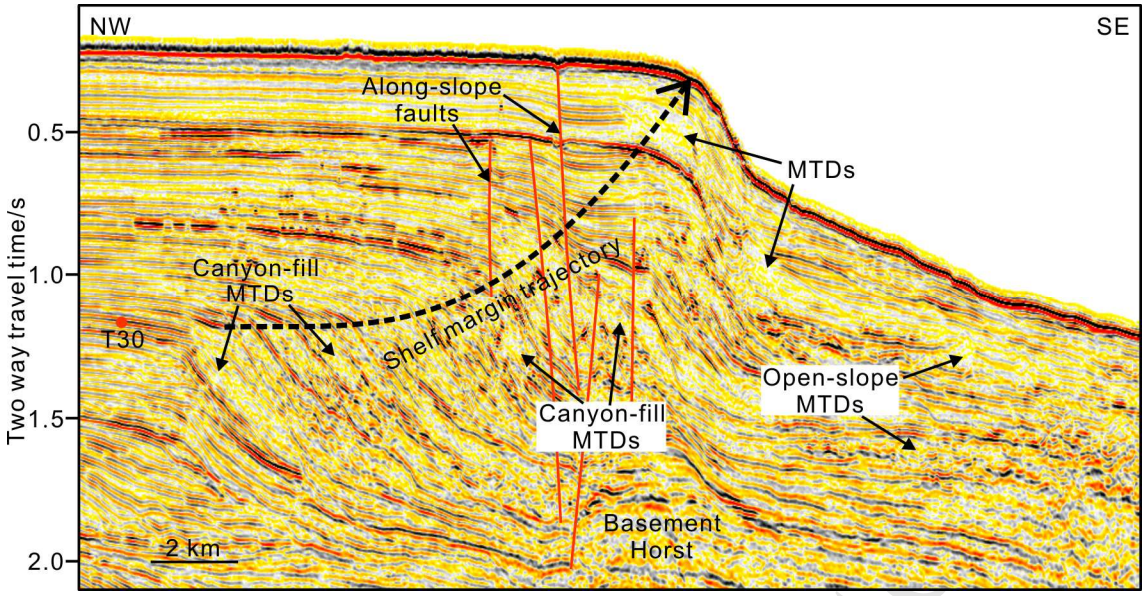

ACCEPTED MANUSCRIPT

ACCEPTED MANUSCRIPT

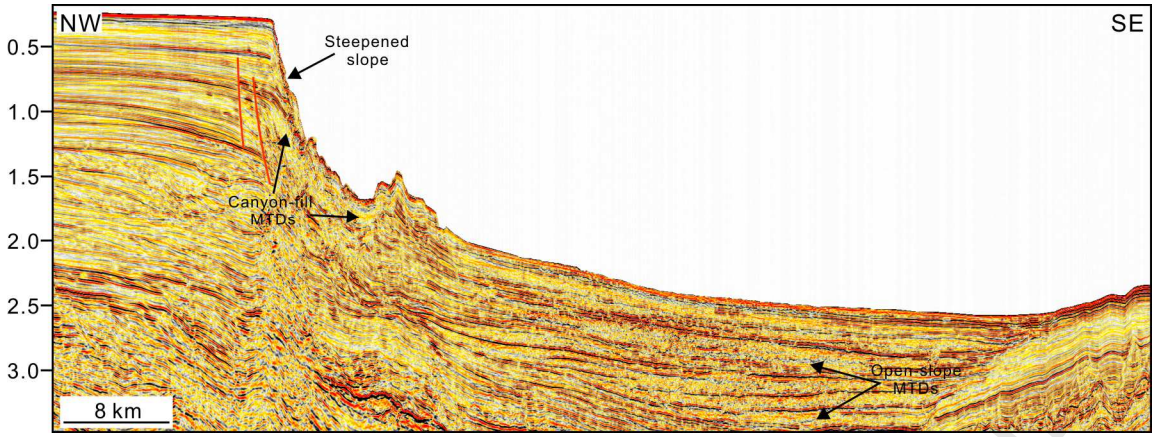

ACCEPTED MANUSCRIPT

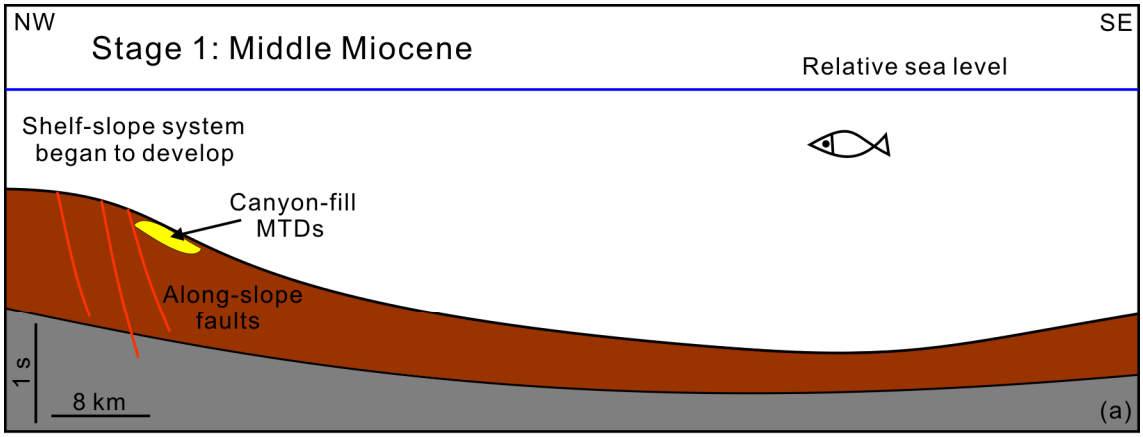
NW
SE
Stage 1: Middle Miocene
Relative sea level
Shelf-slope system
began to develop
Canyon-fill
MTDs
Along-slope
faults
1 s
8 km
(a)

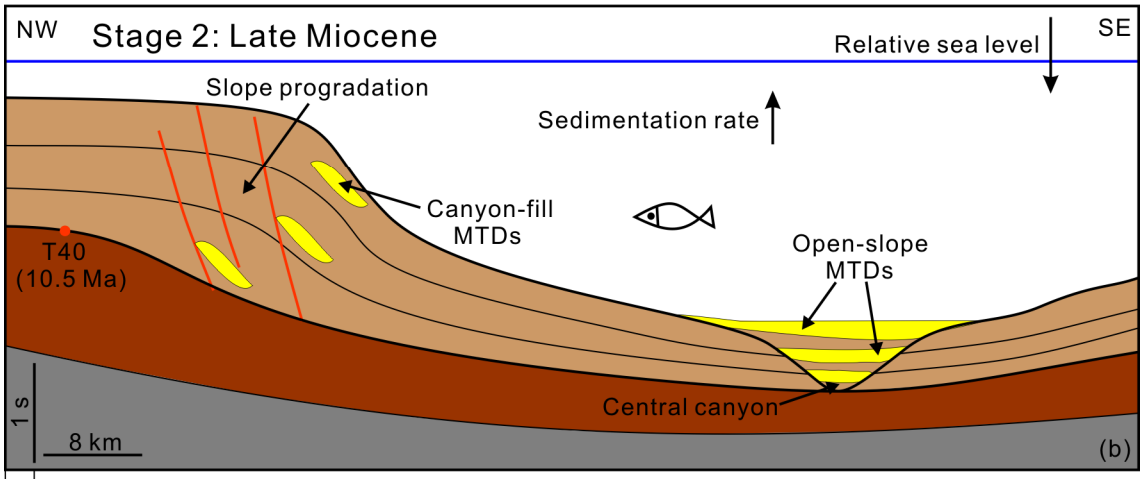
NW
Stage 2: Late Miocene
Relative sea level
SE
Slope progradation
Sedimentation rate
Canyon-fill
MTDs
T40
(10.5 Ma)
Open-slope
MTDs
Central canyon
1 s
8 km
(b)

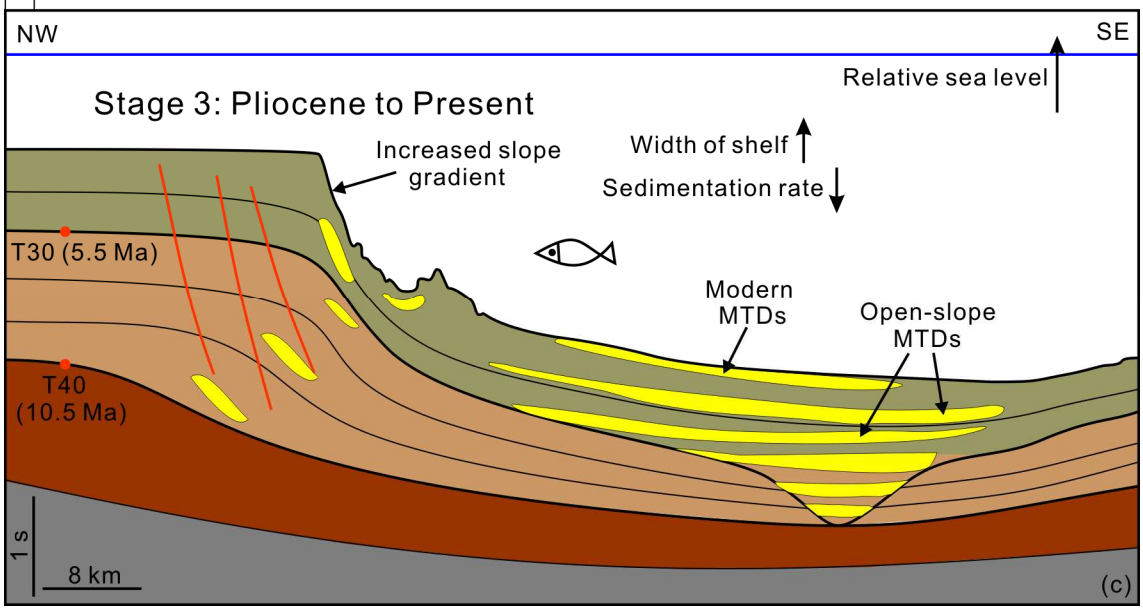
NW
SE
Relative sea level
Stage 3: Pliocene to Present
Increased slope
gradient
Width of shelf
Sedimentation rate
T30 (5.5 Ma)
Modern
MTDs
Open-slope
MTDs
T40
(10.5 Ma)
1 s
8 km
(c)

ACCEPTED MANUSCRIPT

- Strike-slip tectonics resulted in the deposition of seven large MTDs in the South China Sea
- Reservoir potential in submarine channels depends on the nature of MTDs filling them
- Sequence-stratigraphic models are distinct in by-pass margins from published models
- ‘Base-of-slope’ fans are replaced by widespread MTDs on by-pass margins

ACCEPTED MANUSCRIPT